Electronic Supplementary Material (ESI) for Physical Chemistry Chemical Physics.

Supporting information

Engineering Highly Selective CO_2 Electroreduction in Cu-based Perovskites through A-site Cation Manipulation

Shuaibing Yang[a, b], *Xiao-Min Chen*[a, b], *Tao Shao*[b], *Zongnan Wei*[b], *Zhe-ning Chen*[b, c], *Rong Cao*[b, c], *and Minna Cao*[*b, c]

[a] College of Chemistry, Fuzhou University, Fuzhou, 350108, P.R. China

[b] State Key Laboratory of Structural Chemistry, Fujian Institute of Research on the Structure of Matter, Chinese Academy of Sciences, Fuzhou 350002, P.R. China

[c] University of Chinese Academy of Sciences, Beijing 100049, P.R. China

Experimental details

Chemicals.

Lanthanum (III) nitrate hexahydrate ($La(NO_3)_3 \cdot 6H_2O$), Cupric nitrate hydrate ($Cu(NO_3)_2 \cdot 3H_2O$), Cerium (III) nitrate hexahydrate ($Ce(NO_3)_3 \cdot 6H_2O$) and Aqueous ammonia ($NH_3 \cdot H_2O$) were purchased from Sinopharm Chemical Reagent Co., Ltd (China). Citric acid was purchased from Alfa. Strontium carbonate ($SrCO_3$) was purchased from Aldrich. All solutions were prepared with ultrapure water with a resistivity of 18.2 MΩ cm. All reagents were used in their commercially available form without further purification.

Characterization.

X-ray diffraction (PXRD) patterns were collected using a Rigaku Miniflex600 diffractometer equipped with Cu Ka radiation (λ = 1.5406 Å). Scanning Electron Microscope (SEM) images were obtained using a JSM6700-F FESEM. Transmission electron microscope (TEM), high-resolution transmission electron microscope (HR-TEM), high-angle annular dark-filed scanning TEM (HAADF-STEM), and energy dispersive X-ray spectroscopy analysis (EDS) analysis were recorded on a field emission transmission electron microscope (FEI Tecnai F20, 200 kV). Inductively coupled plasma−atomic emission spectroscopy (ICP-AES) measurements were performed on an Ultima 2 analyzer (Jobin Yvon). For the faradaic efficiency analysis, gas products were detected by gas chromatography (Agilent 7820A) equipped with FID and TCD, and liquid products were characterized by ^1H NMR on Bruker AVANCE AV Ⅲ 400. At room temperature, the electrochemical performance measurements were conducted on a CHI1140C electrochemical workstation. The composition and electronic structures of catalysts were analyzed by an ESCALAB 250Xi X-ray photoelectron spectrometer (Thermo Fisher) using an Al Kα source (15 kV, 10 mA). Using an Al Kα as the excitation source, with the pressure inside the chamber maintained below $5.0*10^{-8}$ Pa, the spectra were collected at a pass energy of 40.0 eV. For the accurate comparison of all valence band XPS spectra, the secondary electron background (Smart-type, which is fitted by using Avantage software) was subtracted from the measured spectra. In situ attenuated total reflectance Fourier transform infrared spectroscopy (ATR-FTIR) was obtained by a Nicolet 6700 (Thermo Fisher) equipped with a liquid nitrogen cooled MCT detector. Experiments were in the mixture of 0.1 M $KHCO_3$ and 0.1 M KCl using a homemade ATR-FTIR setup. EIS was measured in CO2-saturated 0.1 M KHCO3 + 0.1 M KCl at -1.4V vs. RHE from 100K Hz to 0.1 Hz.

Supplementary Figures

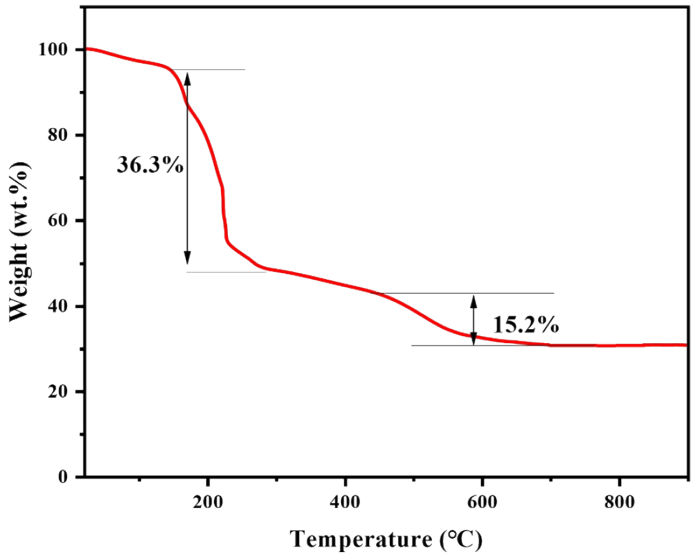

Figure S1. TG curve of La_2CuO_4 precursor.

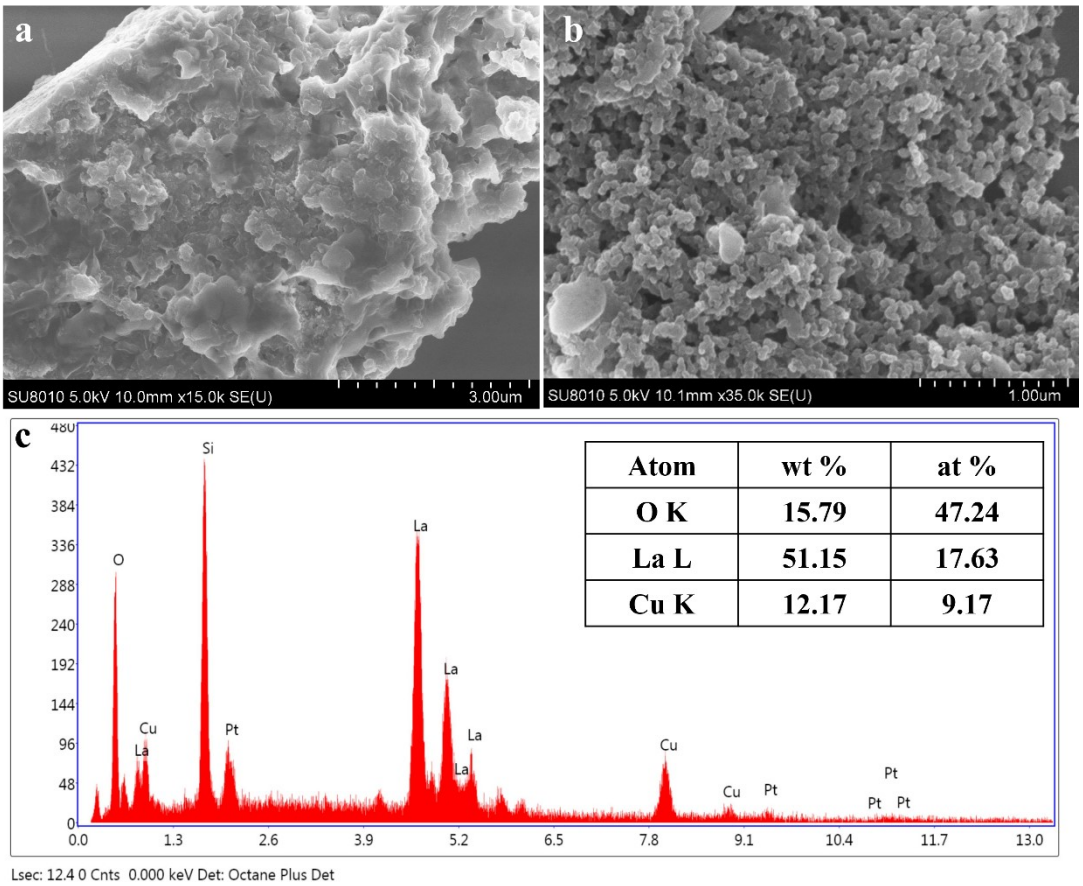

Figure S2. SEM images (scale bar: 3μm a) and 1μm b) and EDS pattern of LCO.

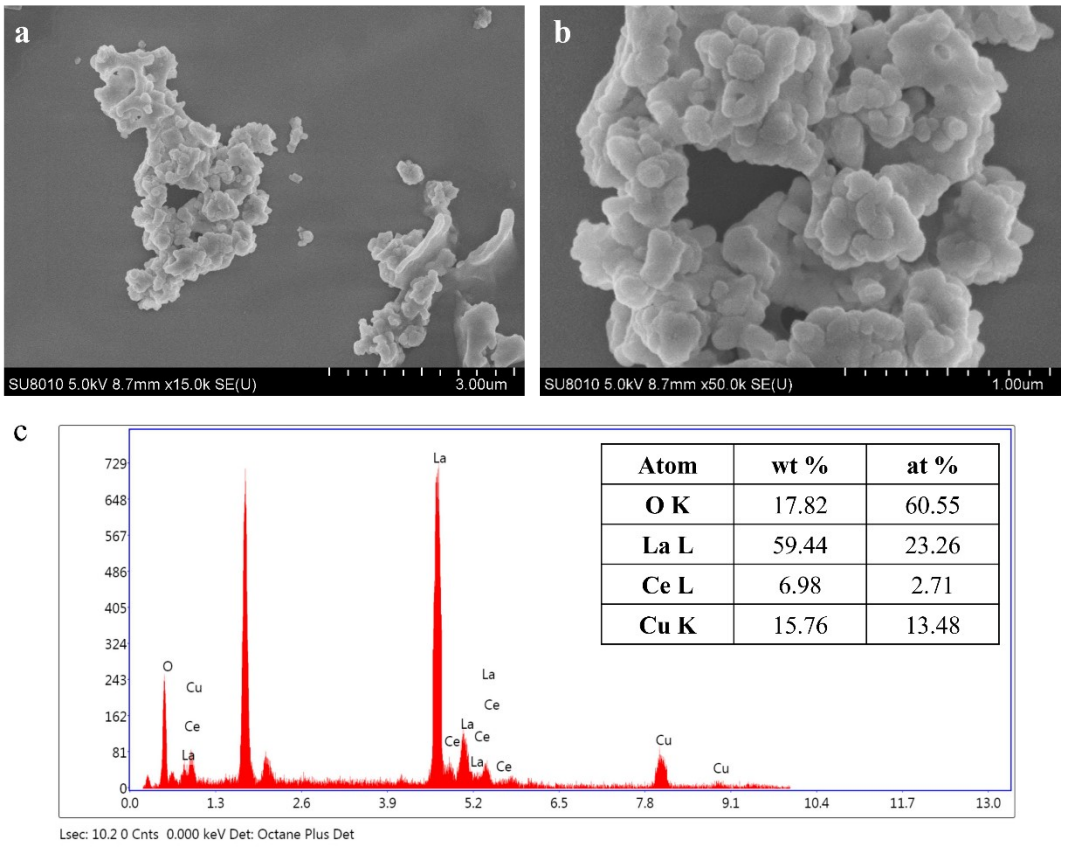

Figure S3. SEM images (scale bar: 3μm a) and 1μm b) and EDS pattern of LCCO.

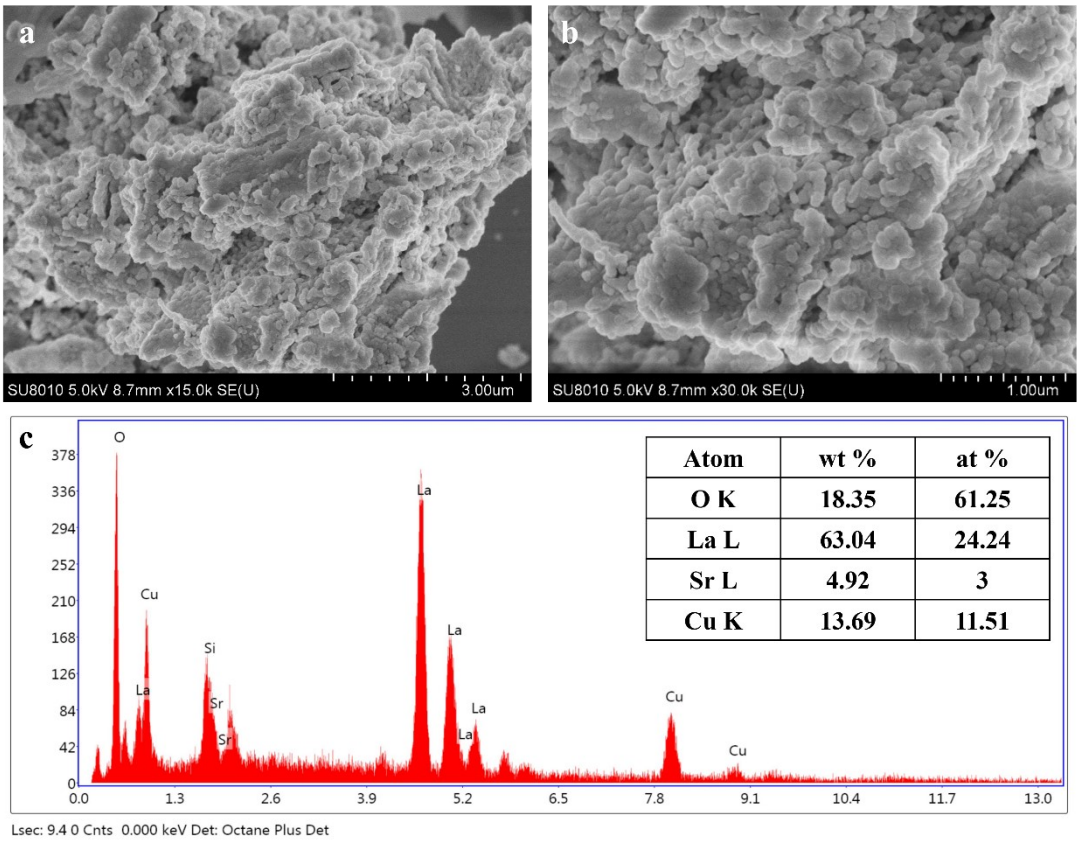

Figure S4. SEM images (scale bar: 3μm a) and 1μm b) and EDS pattern of LSCO.

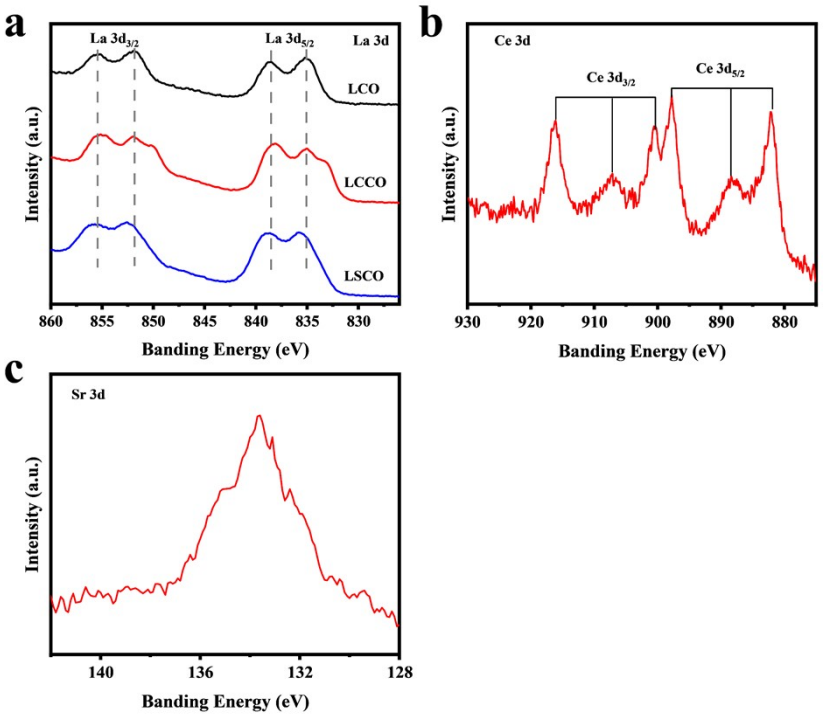

Figure S5. (a) La 3d XPS spectra of LCO, LCCO, and LSCO. (b) Ce 3d XPS spectra of LCCO. (c) Sr 3d XPS spectra of LSCO.

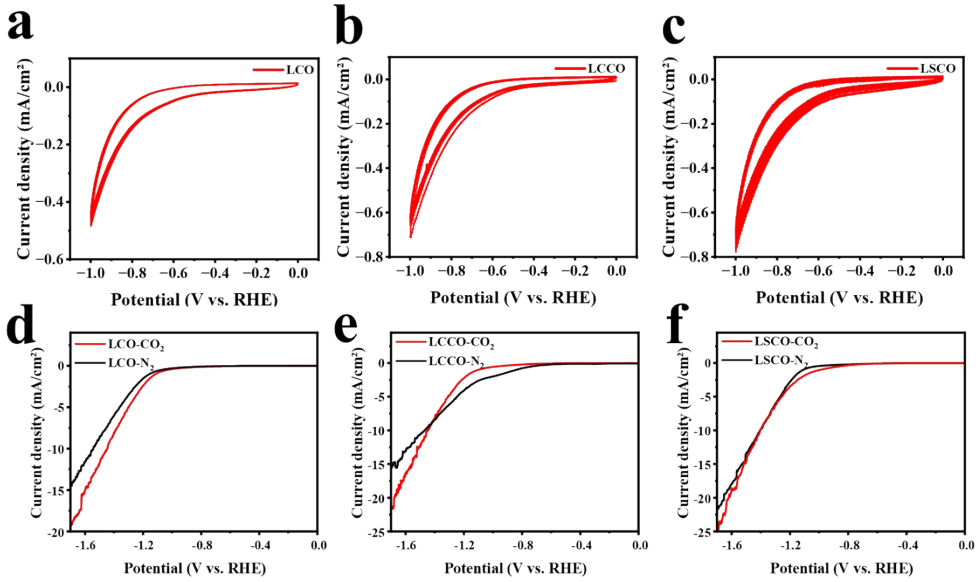

Figure S6. Cyclic voltammetry curves of (a) LCO, (b) LCCO, and (c) LSCO in 0.1M $KHCO_3$ + 0.1M KCl electrolyte. Linear sweep voltammetry curves of (d) LCO, (e) LCCO, and (f) LSCO in saturated CO_2 electrolyte and saturated N_2 electrolyte.

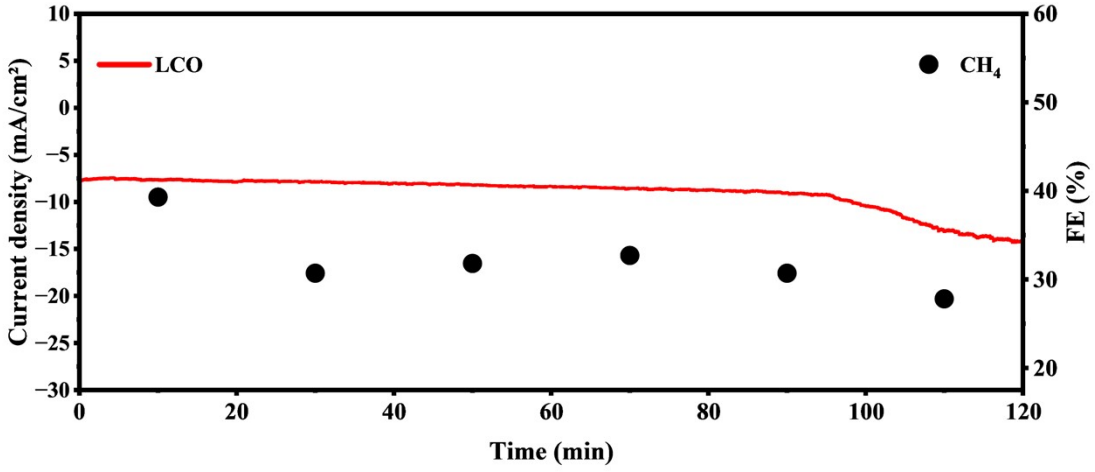

Figure S7. Stability test for CH_4 production over LCO.

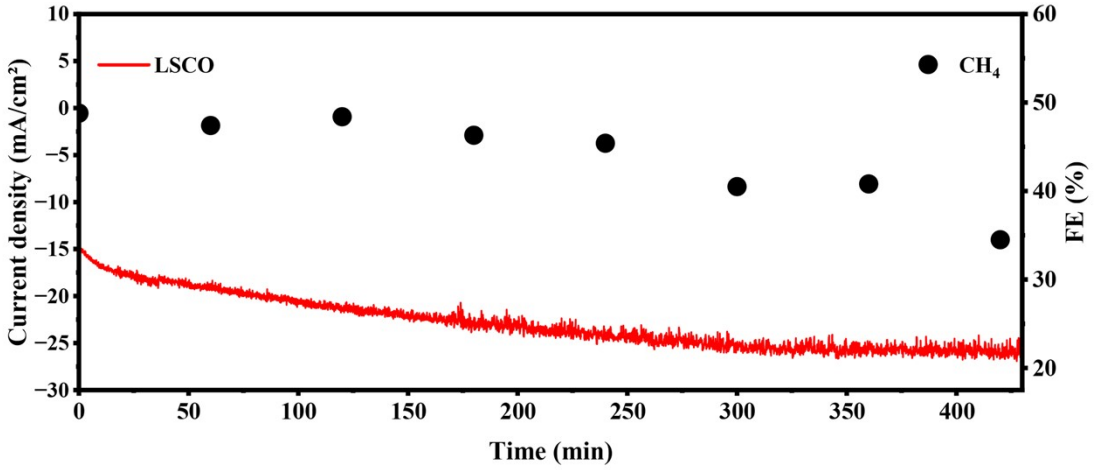

Figure S8. Stability test for CH_4 production over LSCO.

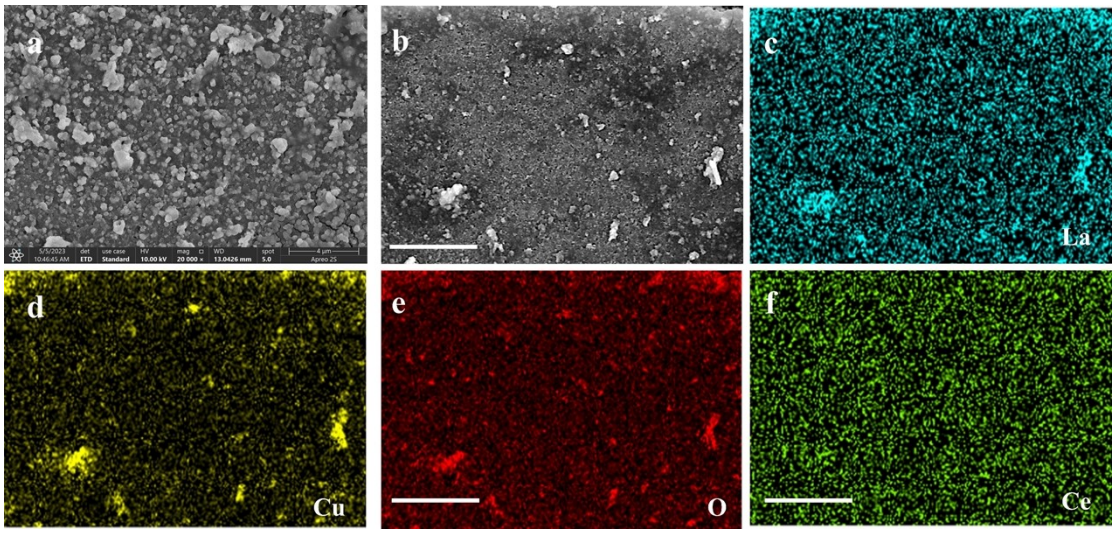

Figure S9. SEM (a), (b), and SEM-EDS elemental mappings of LCCO after durability test (c ~ f)

(Scale bar: 10μm).

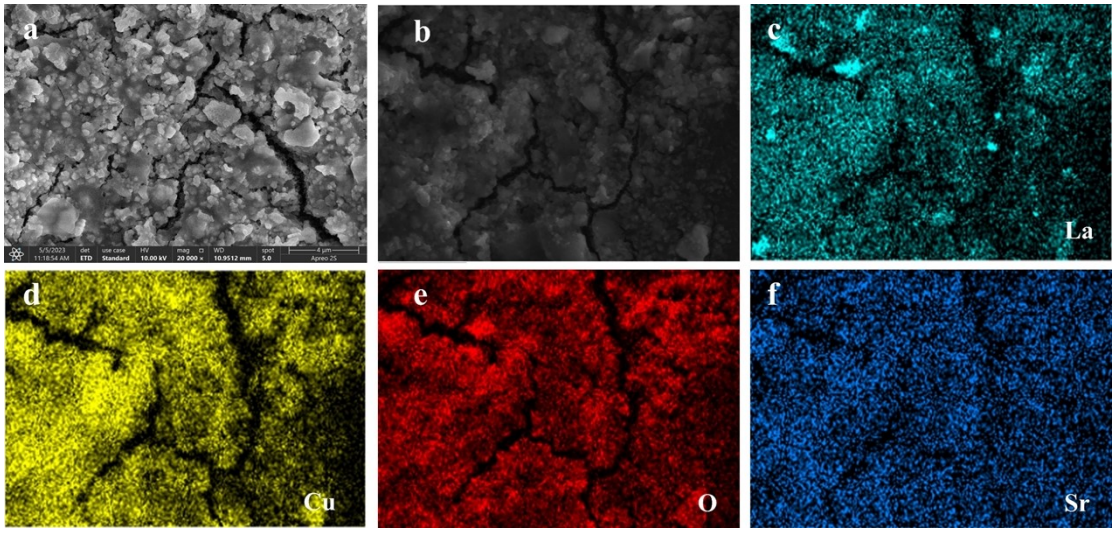

Figure S10. SEM (a), (b), and SEM-EDS elemental mappings of LSCO after durability test (c ~ f) (Scale bar: 10μm).

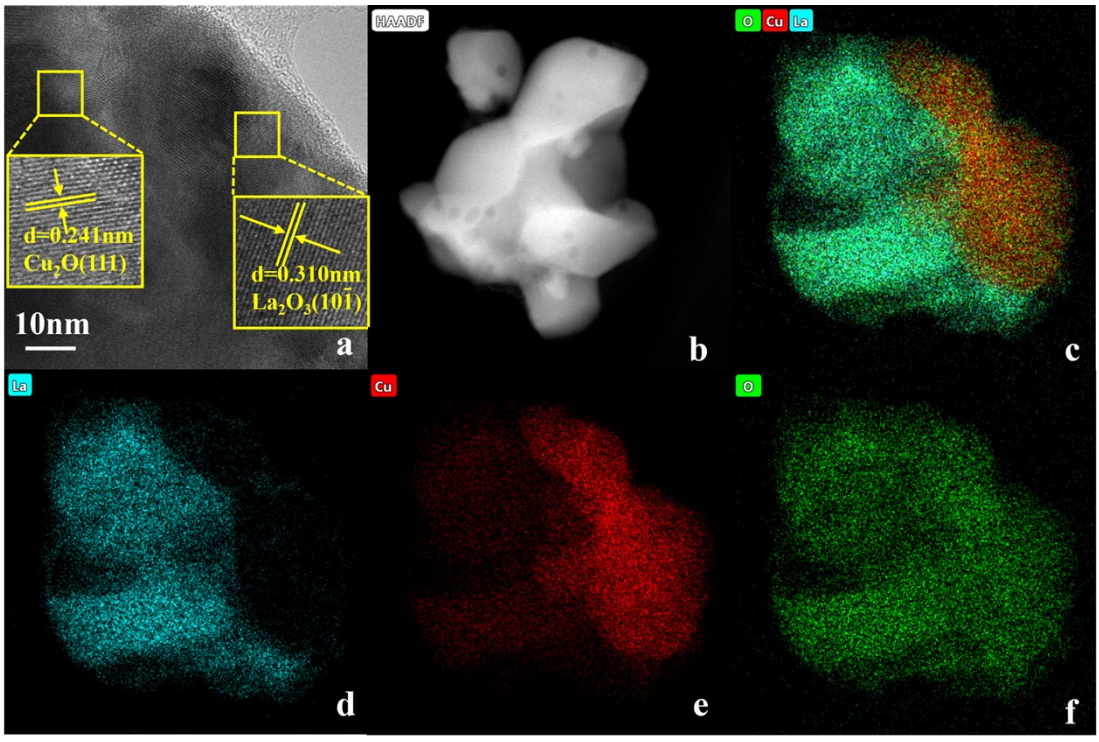

Figure S11. TEM image (a), HAADF-STEM image (b), and the EDX mappings (c ~ f) of LCO after the durability test.

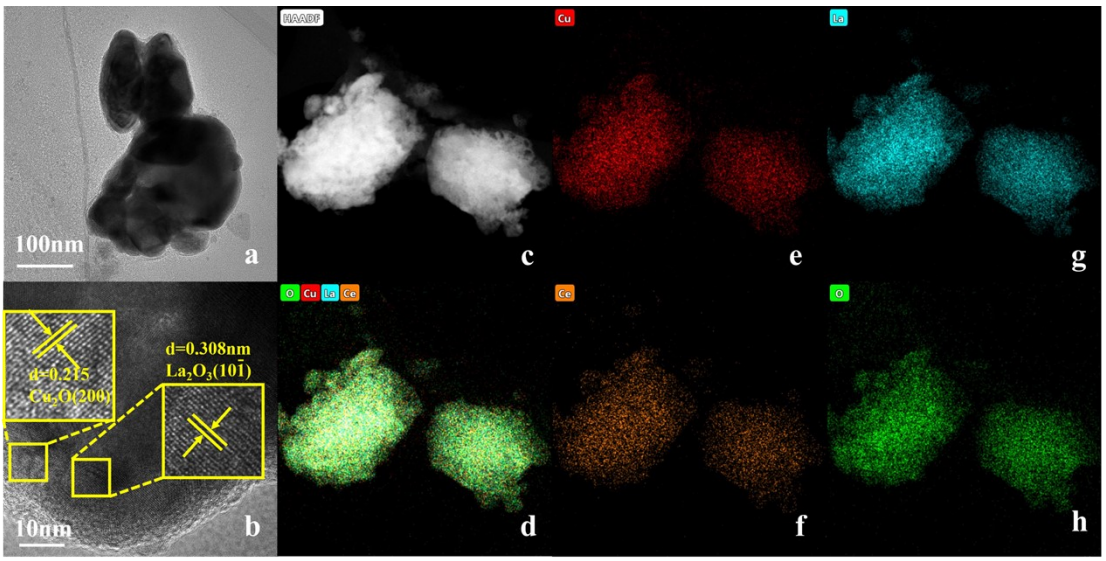

Figure S12. TEM image (a), (b), HAADF-STEM image (c), and the EDX mappings (d ~ h) of LCCO after the durability test.

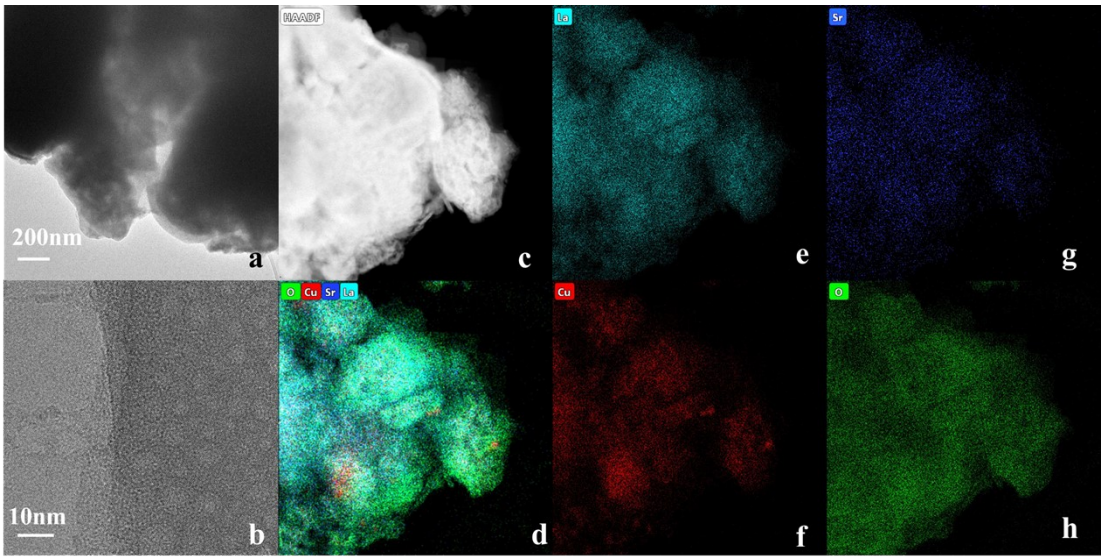

Figure S13. TEM image (a), (b), HAADF-STEM image (c), and the EDX mappings (d ~ h) of LSCO after the durability test.

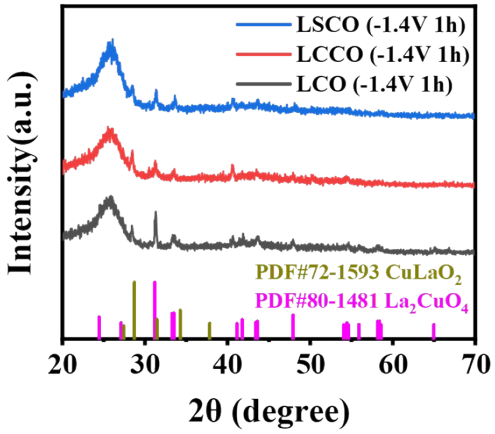

Figure S14. XRD patterns of LCO, LCCO, and LSCO samples after 1h test at -1.4V vs. RHE

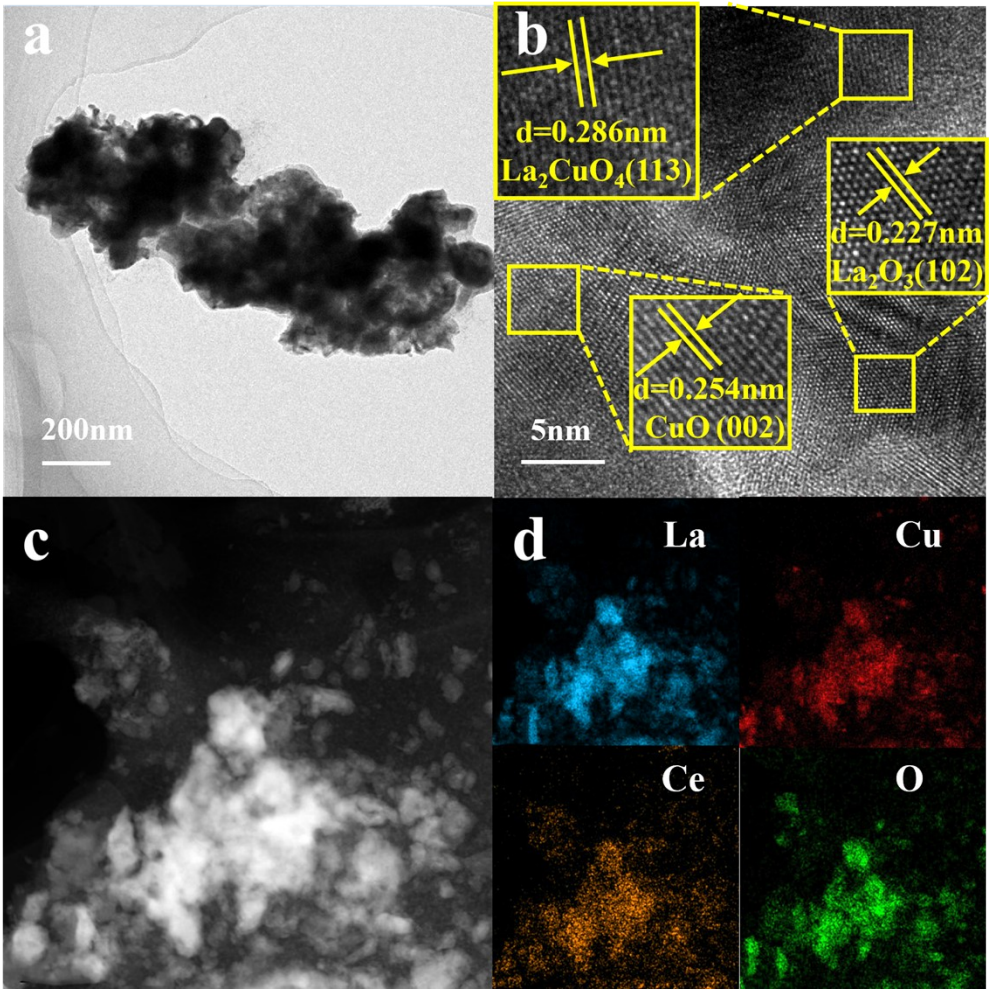

Figure S15. (a) TEM image, (b) HR-TEM, (c) HAADF-STEM image and (d) the EDX mapping of LCCO after 1h test at -1.4V vs. RHE.

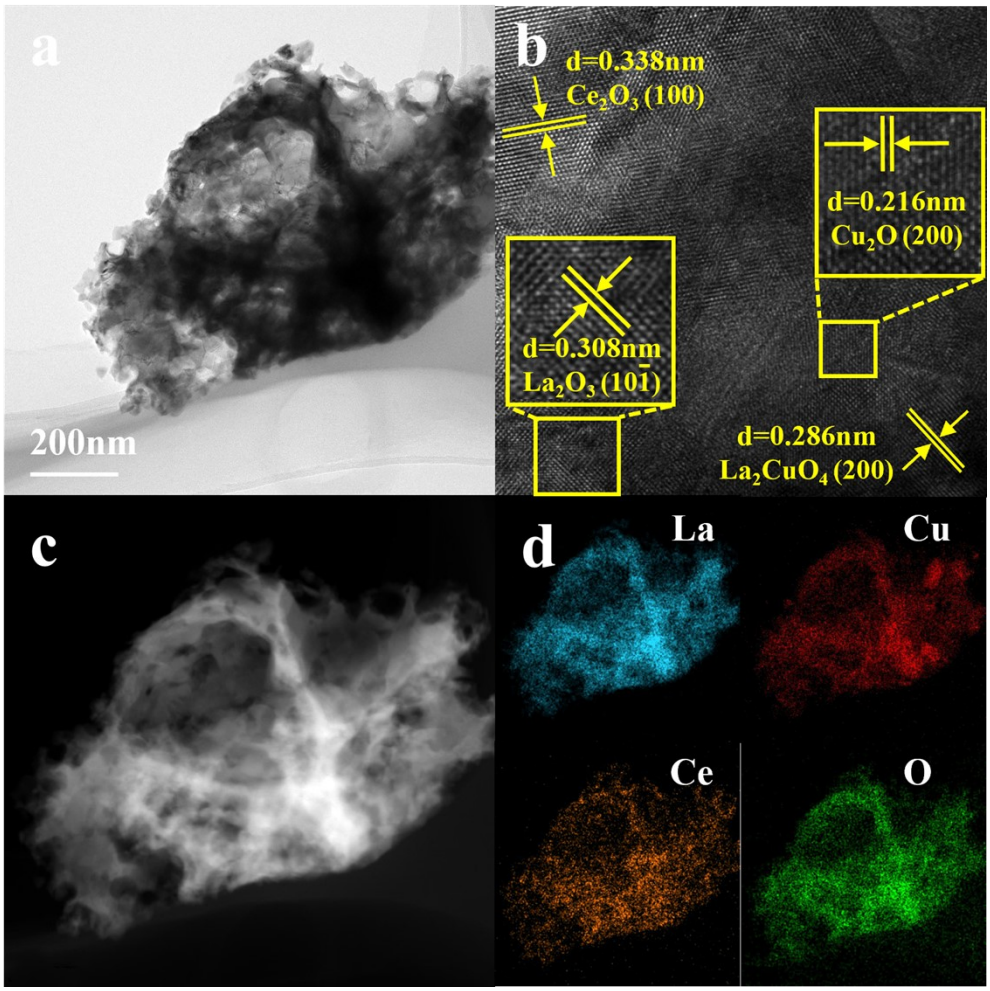

Figure S16. (a) TEM image, (b) HR-TEM, (c) HAADF-STEM image and (d) the EDX mapping of LCCO after 2h test at -1.4V vs. RHE.

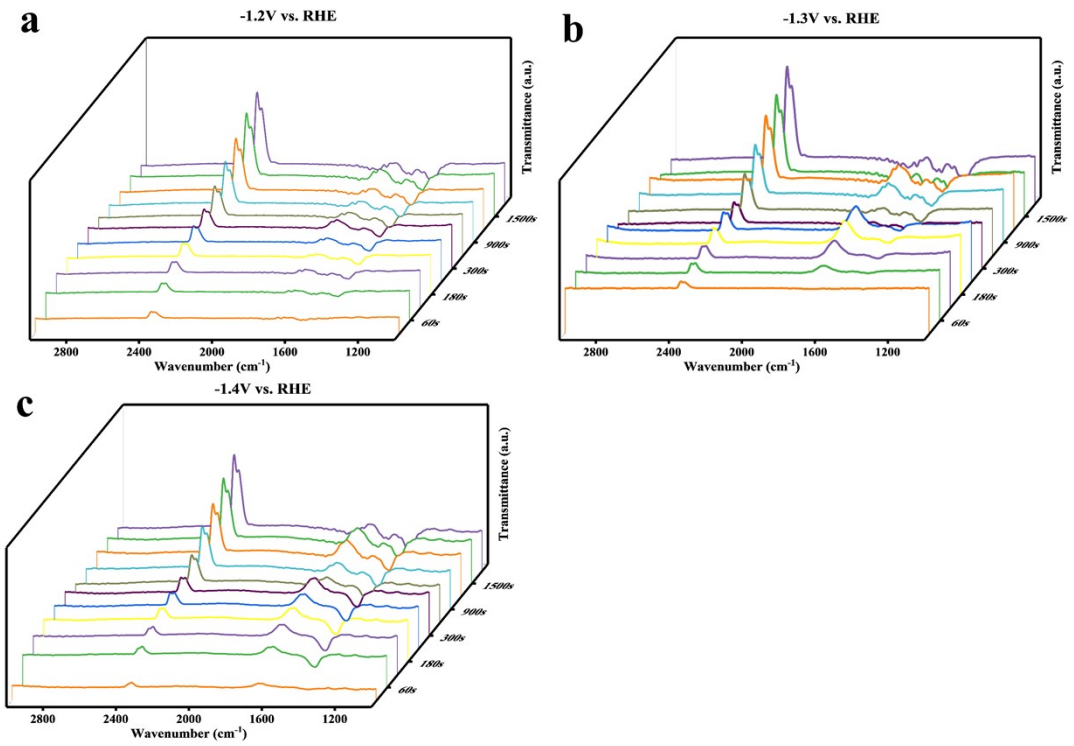

Figure S17. FTIR spectra of LCCO at different voltages and constant voltages at different times. (a) -1.2V vs. RHE, (b) -1.3V vs. RHE, (c) -1.4V vs. RHE.

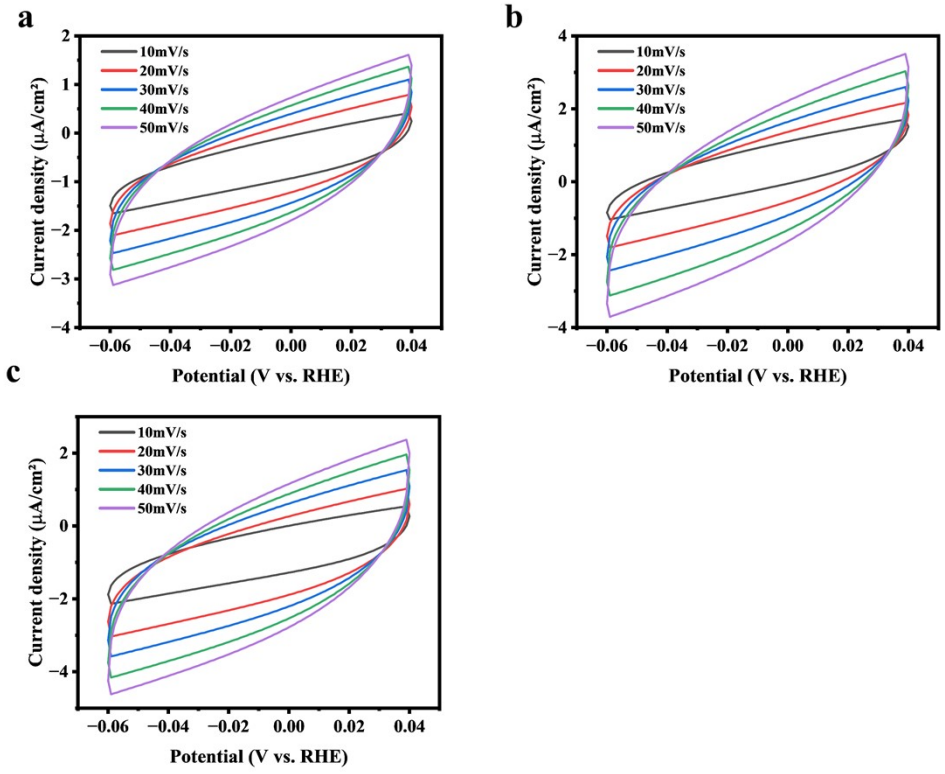

Figure S18. CV curves recorded for the (a) LCO, (b) LCCO, and (c) LSCO catalysts at various scanning rates (i.e., 10, 20, 30, 40, and 50 mV·s^{-1}).

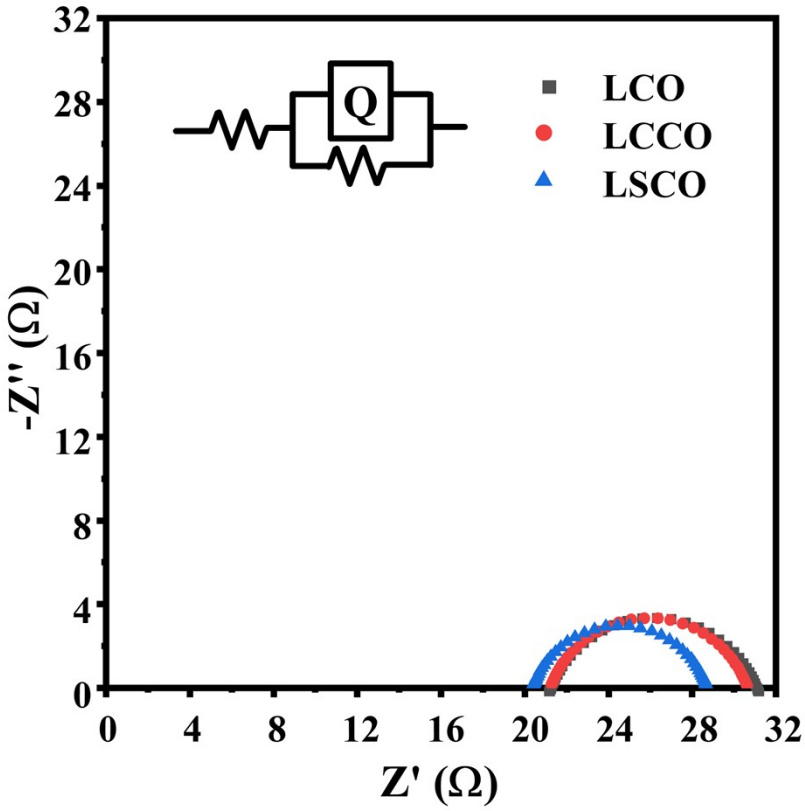

Figure S19. Nyquist plots of the LCO, LCCO, and LSCO catalysts.

Table S1. The atomic composition of LCO, LCCO, and LSCO by ICP-OES

Sample	Weight fraction (%)				Atomic ratio (M/Cu)			
	La	Cu	Ce	Sr	La/Cu	Cu	Ce/Cu	Sr/Cu
LCO	63.05	14.70			1.96	1		
LCCO	55.61	14.43	4.95		1.78	1	0.16	
LSCO	55.87	14.08		4.24	1.82	1		0.21

Table S2. Refined parameters of the LCO, LCCO, and LSCO from Rietveld refinement analysis using the corresponding XRD data.

Name	Space group	Lattice parameters		
		a	b	c
LCO	Fmmm	5.37258	5.4004	13.17735
LCCO	Fmmm	5.34965	5.37294	13.21504
LSCO	Fmmm	5.3556	5.4011	13.149

Table S3. Cu 2p XPS peak fitting parameters for LCO, LCCO, and LSCO

LCO-Cu 2p

Name	Peak position (eV)	FWHM	Peak area
Cu^{2+} $2p_{3/2}$	933.2	3.36	10953.86
Cu^{2+} $2p_{1/2}$	953.0	3.36	5670.08

LCCO-Cu 2p

Name	Peak position (eV)	FWHM	Peak area
Cu^{+} $2p_{3/2}$	932.6	1.95	6899.17
Cu^{2+} $2p_{3/2}$	933.6	2.65	13565.67
Cu^{+} $2p_{1/2}$	952.4	2.96	7515.7
Cu^{2+} $2p_{1/2}$	954.1	4.30	600.70

LSCO-Cu 2p

Name	Peak position (eV)	FWHM	Peak area
Cu^{+} $2p_{3/2}$	932.8	2.60	4603.18
Cu^{2+} $2p_{3/2}$	934.9	3.24	18583.83
Cu^{+} $2p_{1/2}$	953.5	2.60	2382.76
Cu^{2+} $2p_{1/2}$	954.9	3.50	8620.62

Table S4. O 1s XPS peak fitting parameters for LCO, LCCO, and LSCO

LCO-O 1s

Name	Peak position (eV)	FWHM	Peak area
lattice O^{2-}	529.2	1.69	2692.46
Surface-adsorbed O_2	531.4	2.09	38863.4

or hydroxyl groups			
Surface-adsorbed H_2O	533.1	1.24	8474.91

LCCO-O 1s

Name	Peak position (eV)	FWHM	Peak area
lattice O^{2-}	528.7	1.69	25808.89
O_2^{2-}/O^-	530.7	1.54	13306.19
Surface-adsorbed O_2 or hydroxyl groups	531.5	1.53	28047.04
Surface-adsorbed H_2O	532.6	1.90	5847.13

LSCO-O 1s

Name	Peak position (eV)	FWHM	Peak area
lattice O^{2-}	528.8	1.59	14867.02
O_2^{2-}/O^-	530.5	1.32	6601.67
Surface-adsorbed O_2 or hydroxyl groups	531.5	1.67	35947.17
Surface-adsorbed H_2O	532.8	1.73	5071.01

Table S5. Cu^+ ratio in LCO, LCCO, and LSCO calculated by XPS.

Name	Cu^+	Cu^{2+}
LCO	0	1
LCCO	0.336	0.664
LSCO	0.198	0.802